balt3/zbc-bc/zbc-bc/zbc01310/zbc0798-10z ZSUBMIT 18 xppws S=1 21/1/10 7:07 | 4/Color Figure(s) F1,4,10 | ARTNO: M109.020156

THE JOURNAL OF BIOLOGICAL CHEMISTRY VOL. 285, NO. ??, pp. 1–xxx, ???? ??, 2010
© 2010 by The American Society for Biochemistry and Molecular Biology, Inc. Printed in the U.S.A.

High Affinity Anti-inorganic Material Antibody Generation by Integrating Graft and Evolution Technologies

POTENTIAL OF ANTIBODIES AS BIOINTERFACE MOLECULES[*S]

Received for publication, May 12, 2009, and in revised form, December 23, 2009 Published, JBC Papers in Press, December 31, 2009, DOI 10.1074/jbc.M109.020156

Takamitsu Hattori[‡], Mitsuo Umetsu[‡§1], Takeshi Nakanishi[‡], Takanari Togashi[¶], Nozomi Yokoo[¶], Hiroya Abe[‖], Satoshi Ohara[‖], Tadafumi Adschiri[¶], and Izumi Kumagai[‡2]

From the [‡]Department of Biomolecular Engineering, Graduate School of Engineering, Tohoku University, Sendai 980-8579, the [§]Center for Interdisciplinary Research, Tohoku University, Sendai 980-8578, the [¶]Institute of Multidisciplinary Research for Advanced Materials, Tohoku University, Sendai 980-8577, and the [‖]Joining and Welding Research Institute, Osaka University, Osaka 567-0047, Japan

Recent advances in molecular evolution technology enabled us to identify peptides and antibodies with affinity for inorganic materials. In the field of nanotechnology, the use of the functional peptides and antibodies should aid the construction of interface molecules designed to spontaneously link different nanomaterials; however, few material-binding antibodies, which have much higher affinity than short peptides, have been identified. Here, we generated high affinity antibodies from material-binding peptides by integrating peptide-grafting and phage-display techniques. A material-binding peptide sequence was first grafted into an appropriate loop of the complementarity determining region (CDR) of a camel-type single variable antibody fragment to create a low affinity material-binding antibody. Application of a combinatorial library approach to another CDR loop in the low affinity antibody then clearly and steadily promoted affinity for a specific material surface. Thermodynamic analysis demonstrated that the enthalpy synergistic effect from grafted and selected CDR loops drastically increased the affinity for material surface, indicating the potential of antibody scaffold for creating high affinity small interface units. We show the availability of the construction of antibodies by integrating graft and evolution technology for various inorganic materials and the potential of high affinity material-binding antibodies in biointerface applications.

AQ: A

Peptides and proteins recognize the interfacial surfaces of their corresponding molecules with high affinity and selectivity because of the multiple-point interactions of hydrogen bonds and salt bridges and the surficial complementarities at the interfaces. Surface recognition by proteins has also been observed in biopolymers in biological systems (1, 2). Furthermore, the use of recent combinatorial library approaches has enabled the identification of short peptides with affinity for nonbiological inorganic materials (3–5). Peptides that bind materials such as metals, metal oxides, and semiconductors have been identified, and they are expected to be useful in bottom-up fabrication procedures in the field of bio-nanotechnology, such as patterning and assembly of proteins and nanomaterials (6–8), biofunctionalization of nanoparticles (9, 10), and synthesis of crystalline nanometer-sized metal particles (11, 12).

Besides short peptides, antibodies are becoming attractive as novel material-binding molecules because they have higher affinities and specificities than peptides. Antibodies are recognition molecules with high binding affinity and specificity in the immune system, and they have been used widely in the fields of medical and analytical chemistry (13). By the use of general methodologies with *in vivo* immune system and *in vitro* combinatorial selection technologies, antibodies to the surfaces of organic crystals of 1,4-dinitrobenzene (14) and tripeptide (15), magnetite (16), gallium arsenide (17), gold (18), and polyhydroxybutyrate (19) have been identified in immunized mice or in libraries of naturally occurring human antibodies. These results demonstrate the potential of antibodies for recognizing the solid surfaces of bulk materials. However, far fewer material-binding antibodies have been obtained than peptides, because the immunogenic potential of solid materials is not high and the vertebrate immune system is not strongly sensitized by such materials. Even if *in vitro* selection methods are used, the limited library diversity and the strong nonspecific interactions of coat proteins on phages with solid bulk surfaces make selecting positive antibodies difficult.

Here, we generated high affinity antibodies against zinc oxide (ZnO), aluminum oxide (Al_2O_3), and cobalt oxide (CoO) material surfaces by the integration of peptide-grafting and evolutional technologies (Fig. 1). We first grafted a peptide sequence with affinity for the surface of an inorganic material into a CDR[3] loop of the single variable domain of the heavy chain of a heavy

F1

Fn3

* This work was supported by a scientific research grant from the Ministry of Education, Science, Sports and Culture of Japan (to M. U. and I. K.), the Industrial Technology Research Grant Program 2005 of the New Energy and Industrial Technology Development Organization of Japan (to M. U.), proposal-oriented research promotion program of Japan Science and Technology of Japan (to M. U.), Japan Society for the Promotion of Science research fellowships for young scientists (to T. H.), and in part by The Hosokawa Foundation (to M. U.).

[S] The on-line version of this article (available at http://www.jbc.org) contains supplemental Tables S1–S5 and Fig. S1.

ZSI

[1] To whom correspondence may be addressed: Aoba 6-6-11-608; Aoba-ku, Sendai 980-8579, Japan. Tel.: 81-22-795-7276; Fax: 81-22-795-7276; E-mail: mitsuo@kuma.che.tohoku.ac.jp.

[2] To whom correspondence may be addressed: Aoba 6-6-11-606, Aoba-ku, Sendai 980-8579, Japan. Tel.: 81-22-795-7274; Fax: 81-22-795-6164; E-mail: kmiz@kuma.che.tohoku.ac.jp.

[3] The abbreviations used are: CDR, complementarity determining region; Fv, variable fragment of antibody; GdnHCl, guanidine hydrochloride; VHH, variable domain of heavy chain of heavy chain antibody; ZnOBP, ZnO-binding peptide; sZnOBP, selected ZnO-binding peptide; GFP, green fluorescent protein.

High Affinity Anti-inorganic Material Antibody Generation

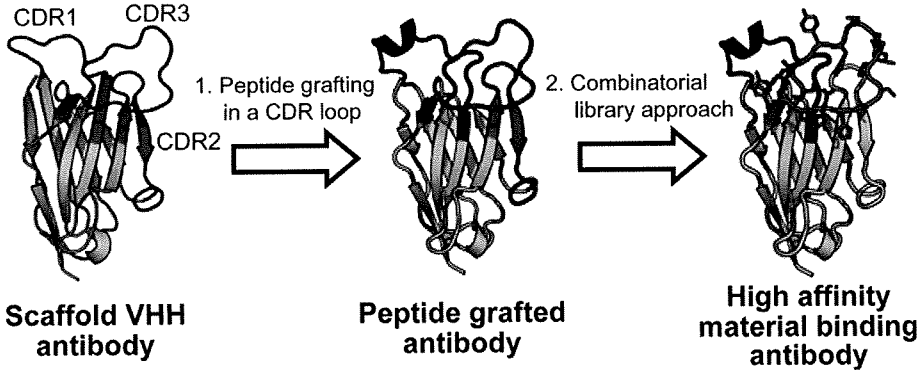

FIGURE 1. **Construction of antibody by integrating grafting and evolutionary technologies.**

chain camel antibody (VHH) to give a VHH fragment with the same affinity as the grafted peptide and without structural instability. Next, a nonrelated CDR loop in the peptide-grafted VHH was randomized by using an $\alpha\beta\beta\alpha$ motif sequence (see under "Results") to screen for high affinity antibodies. Application of the single-domain VHH fragment as a framework prevented destabilization in the grafting of the alien peptide in the first step, and construction of a VHH library from the peptide-grafted VHH fragment by using the $\alpha\beta\beta\alpha$ motif sequence enabled us to bypass limitations on library diversity. We also demonstrate the enthalpy synergistic effect from grafted and selected CDR loops on the binding mechanism of antibodies onto material surfaces and the potential of antibody scaffold for creating high affinity small interface units.

EXPERIMENTAL PROCEDURES

Construction of Expression Vectors for VHH Fragment with Material-binding Peptide in CDRs—The DNA sequences coding the VHH fragments of camel anti-BclI β-lactamase antibody cAbBCII10 (20) were synthesized from five oligonucleotides and external primers (supplemental Table S1) by means of overlap extension PCR with LA-Taq DNA polymerase (21). The gene fragments produced were inserted into the NcoI-SacII site of par-FLAG vectors containing a FLAG peptide sequence, as constructed previously (22), to produce plasmids for the cAbBCII10 VHH fragment with a FLAG sequence at the C terminus (pRA-wtVHH-FLAG).

The DNA sequences coding the VHH fragment where the CDR loops were replaced with ZnO-, Al_2O_3-, or CoO-binding peptides (11, 23, 24) were generated by means of overlap extension PCR from plasmid pRA-wtVHH-FLAG, using the oligonucleotides and external primers shown in supplemental Table S2. The amplified sequences for the VHH fragments were inserted into the NcoI-SacII sites of the pRA-FLAG vectors to produce the pRA-VHH-FLAG plasmids. For the VHH with a material-binding peptide at the N terminus, the DNA sequences were amplified from the pRA-wtVHH-FLAG plasmid by using the primers in supplemental Table S2 and then inserted into the NcoI-SacII fragment of the pRA-FLAG vector.

Construction of VHH Phage Library and Selection of VHH with High Affinity for Material Surfaces—DNA sequences encoding the VHH_{ZnOBP1}, VHH_{AlOBP1}, and VHH_{CoOBP1} fragments with randomized sequences in the CDR 3 loop were generated and amplified from the pRA-VHH-FLAG plasmids with each peptide-grafted VHH by using the primers in supplemental Table S3 and overlap extension PCR. The amplified sequences for VHH were inserted into the NcoI-SacII fragment of the phagemid vector of pTZ-PsFv2, which was constructed for phage display of the HyHEL-10 variable fragment (25), to display the VHH fragments on the filamentous bacteriophage M13. For the selection of VHH with high affinity for inorganic materials, ~10^9 phages were mixed with 0.2 mg of material particles about 100 nm in diameter (ZnO, Hosokawa Micron Inc., Hirakata, Japan), 200 nm in diameter (Al_2O_3, Taimei Chemicals Co., Ltd., Nagano, Japan), and 40 nm in diameter (CoO, C.I. Kasei Co., Ltd., Tokyo, Japan) in a 10 mM phosphate solution, pH 7.5, with 200 mM NaCl and 0.05% Tween 20 at room temperature for 1 h. The particles were then washed with 10 mM phosphate buffer to remove unbound phages. The residual phages bound to the particles were separated with 200 or 500 mM phosphate solution (200 mM for ZnO and 500 mM for CoO and Al_2O_3), and then the eluted phages were amplified in *Escherichia coli* JM 109 as described previously (25). This panning procedure was performed a total of four times, with increases in the phosphate concentration of the washing solution to 30–50 mM to select the phages displaying antibodies with high affinity for target material surface. After four rounds of selection, the amino acid sequences of the VHH displayed on the isolated phage were analyzed in 200 randomly isolated phage clones. Selected VHH genes were inserted into the NcoI-SacII fragment in the pRA-FLAG vector to express the encoding VHH fragments in *E. coli*.

Using one of the selected VHH genes (4F2 clone), we further prepared the DNA sequences of the selected VHH fragment with CDR 1 loop exchanged for that of cAbBCII10 to evaluate the role of the CDR 3 sequence in selected VHH. The sequences coding the VHH fragment with CDR 1 of cAbBCII10 and CDR 3 of 4F2 VHH were generated by means of overlap extension PCR from plasmid pRA-FLAG vector with the 4F2 VHH gene, using the two oligonucleotides and external primers shown in supplemental Table S4, and the amplified sequences for the VHH fragments were inserted into the NcoI-SacII sites of the pRA-FLAG vectors to produce the pRA-$VHH_{sZnOBP3}$-FLAG plasmids.

Expression and Purification of VHH Fragments—Transformed *E. coli* BL21 (DE3) cells harboring the expression plasmid encoding VHH fragments were incubated in lysogeny broth medium at 28 °C, and expression of antibody fragments under the control of the T7 promoter was induced by adding 1 mM isopropyl β-D-thiogalactopyranoside. VHH fragments were extracted from the periplasm of the harvested cells by osmotic shock and purified by anion/cation exchange and gel filtration chromatographies after ammonium sulfate treatment.

balt3/zbc-bc/zbc01310/zbc0798-10z ZSUBMIT 18 xppws S=1 21/1/10 7:07 | 4/Color Figure(s) F1,4,10 | ARTNO: M109.020156

Analysis of Binding Affinities of Antibody Fragments to Material Surfaces—Material particles (0.2 mg) with a Brunauer-Emmett-Teller (BET) specific surface area (surface area estimated by nitrogen gas adsorption (26)) of 9.7 m^2/g (ZnO), 12.4 m^2/g (Al_2O_3), 30.9 m^2/g (CoO), 33.9 m^2/g (Fe_2O_3, C. I. Kasei Co., Ltd., Tokyo, Japan), 39.1 m^2/g (TiO_2,C. I. Kasei Co., Ltd., Tokyo, Japan), or 39.8 m^2/g (NiO, C.I. Kasei Co., Ltd.) were separately added to 300 μl of 10 mM phosphate solution (pH 7.5; 200 mM NaCl, 0.05% Tween 20) containing VHH, and the mixture was incubated for 30 min at several temperatures. After centrifugation at 20,000 × *g* for 10 min, the precipitated particles were added to 300 μl of 6 M guanidine hydrochloride (GdnHCl) solution (10 mM phosphate, 200 mM NaCl, pH 7.5) to elute the adsorbed proteins from the particles. The supernatants were analyzed by SDS-PAGE, and the proteins eluted were quantified with a MicroBCA protein assay reagent kit (Pierce).

Competitive Inhibition Assay for the Binding of VHH onto ZnO with ZnO-binding Peptides—ZnO particles (0.2 mg) were added to 300 μl of a 10 mM phosphate solution containing 3 μM VHH (pH 7.5; 200 mM NaCl, 0.05% Tween 20), and the mixture was incubated for 30 min at 4 °C. After centrifugation at 20,000 × *g* for 10 min, the precipitated ZnO particles were washed with 10 mM phosphate solution to remove nonspecifically adsorbed VHH. After removing the washing solution, the particles were suspended in 300 μl of 10 mM phosphate solutions containing the ZnO-binding peptides at 3 μM, and the suspension was centrifuged at 20,000 × *g* for 10 min. This inhibition procedure was repeated until the concentration of peptides was increased to 3 mM, and all the supernatants were analyzed by SDS-PAGE. Residual VHH on ZnO particle even after the inhibition procedure with 3 mM peptides were eluted with 6 M GdnHCl solution, and the supernatant was also analyzed by SDS-PAGE.

Construction of Bispecific VHH Dimers with Affinity for ZnO Surface and GFP—The sequence of anti-GFP VHH (cAbGFP4) (27) was generated from five oligonucleotides and two external primers (supplemental Table S5) by means of overlap extension PCR with LA-Taq DNA polymerase, and the gene fragments were inserted into the NcoI-SacII site of the pRA-FLAG vectors to product the plasmids (pRA-cAbGFP4-FLAG). To generate bispecific antibody with affinity for ZnO and GFP, the gene sequence of cAbGFP4 was fused at the C terminus of 4F2 VHH via a llama IgG2 upper hinge-linker (EPKIPQPQPKPQPQPQPQPQPKPQPKPEP) (28). The gene sequence was generated and amplified from the plasmids of pRA-4F2VHH-FLAG and pRA-cAbGFP4-FLAG by using the primers in supplemental Table S5, and the amplified gene fragments were inserted into the NcoI-SacII fragment of the pRA-FLAG vector (4F2 VHH-llama IgG2 upper hinge linker-cAbGFP4). The bispecific VHH dimers were expressed in *E. coli* and prepared as for the other VHH fragments.

Reflectometric Interference Spectroscopy—A biosensor array system with reflectometric interference spectroscopy (Fluidware Technology Inc., Kawaguchi, Japan) was used to measure the binding of VHH fragments to ZnO films and the bispecificity of VHH dimers. VHH monomer or bispecific VHH dimer (1 μM) in 10 mM phosphate buffer (pH 7.5; 200 mM NaCl) was directly flowed for 240 s onto a ZnO film deposited on a silicon plate at the flow rate of 10 μl/min, and the change in wavelength with minimum reflection intensity was measured. For bispecific VHH dimers, 1 μM GFP was further injected after washing with 10 mM phosphate buffer for 240 s.

TABLE 1
Amino acid sequences of CDR loops of ZnOBP-grafted VHH fragments
ZnO-binding peptide is underlined. Numbering of the amino acids of cAbBCII10 VHH follows the Kabat numbering system (20). Amino acids of ZnOBP-grafted VHH are numbered as 1–1 to 1–18 (CDR 1 in VHH_{ZnOBP1}), 2–1 to 2–20 (CDR 2 in VHH_{ZnOBP2}), and 3–1 to 3–16 (CDR 3 in VHH_{ZnOBP3}).

Fragment	Sequence of CDR 1	Sequence of CDR 2	Sequence of CDR 3
	26 35c	50 65	95 102
cAbBCII10	GGSEYS-YSTFSLG	AIASM--GGLTYYADSVK-G	VRGYFMRLPSSHNFRY
	1-1 1-18	50 65	95 102
VHH_{ZnOBP1}	GGSEAHVMHKVAPRPSLG	AIASM--GGLTYYADSVK-G	VRGYFMRLPSSHNFRY
	26 35c	2-1 2-20	95 102
VHH_{ZnOBP2}	GGSEYS-YSTFSLG	AIAEAHVMHKVAPRPDSVK-G	VRGYFMRLPSSHNFRY
	26 35c	50 65	3-1 3-16
VHH_{ZnOBP3}	GGSEYS-YSTFSLG	AIASM--GGLTYYADSVK-G	VEAHVMHKVAPRPFRY

RESULTS

Design for Grafting ZnO-binding Peptide Sequences into CDR Loops of VHH Fragments—As a scaffold for the VHH fragment, we used the camel anti-BcII β-lactamase antibody cAbBCII10, which has an appropriate framework for CDR replacements (20). Table 1 shows the CDR amino acid sequences of VHH with ZnO-binding peptide (ZnOBP; EAHVMHKVAPRP) (11) in CDR 1 (VHH_{ZnOBP1}), CDR 2 (VHH_{ZnOBP2}), and CDR 3 (VHH_{ZnOBP3}). For grafting of ZnOBP into each CDR, we drew upon the crystal structure of the chimera of cAbBCII10 where the CDRs were replaced with those of cAbLys3 (20). In the crystal structure, the N-terminal side of CDR 2 and the C-terminal sides of CDRs 1 and 3 form β structures with the adjacent framework sequences; this has been observed in most reported VHH structures (29, 30). We preserved the edge sequences of the CDRs when the CDR loops were replaced with the ZnOBP sequence.

The crystal structure of ungrafted cAbBCII10 VHH was reported recently (31). It resembles that of the chimeric cAbBCII10; consequently, we confirmed that our grafting design suited the crystal structure of ungrafted cAbBCII10 VHH.

Structure and Binding Ability of VHH Fragments with ZnO-binding Peptide Sequence Grafted in Their CDR Loops—All the ZnOBP-grafted VHH fragments were expressed as soluble forms in *E. coli*, although the VHH_{ZnOBP2} fragments were expressed mainly as insoluble aggregates (data not shown). Analysis of VHH_{ZnOBP1} and VHH_{ZnOBP3} by size-exclusion chromatography and examination of circular dichroism spectra demonstrated a monomeric form with the typical immunoglobulin structure of camel antibody (Fig. 2). However, VHH_{ZnOBP2} formed oligomers with a random structure. Grafting of the peptide sequences into CDR 1 or CDR 3 resulted in little structural change in the framework, but grafting into CDR 2 led to deformation of the camel-type immunoglobulin structure. Reports of the conformational structures of VHH indicate

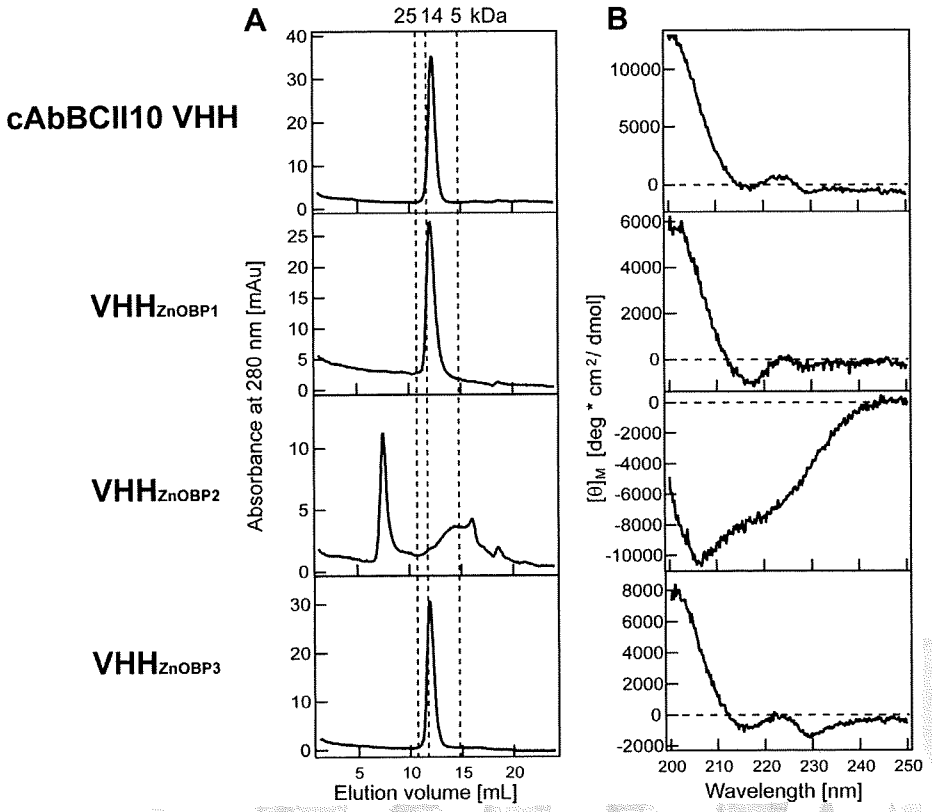

FIGURE 2. *A*, size-exclusion chromatography for cAbBCII10 VHH, VHH_{ZnOBP1}, VHH_{ZnOBP2}, and VHH_{ZnOBP3}. Each 250-μl sample was applied to a Superdex 75 10/300 GL column, and the absorbance of the eluant was monitored at a wavelength of 280 nm. *B*, circular dichroism spectra for the ZnOBP-grafted VHH fragments of cAbBCII10 VHH, VHH_{ZnOBP1}, VHH_{ZnOBP2}, and VHH_{ZnOBP3}.

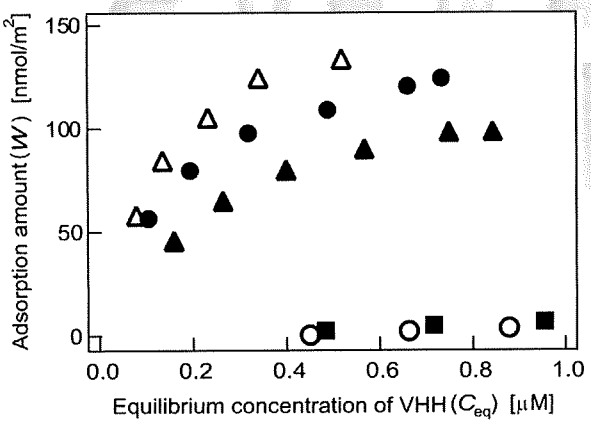

FIGURE 3. **Adsorption isotherms for cAbBCII10 VHH (*open circles*), VHH_{ZnOBP1} (*closed circles*), VHH_{ZnOBP3} (*closed squares*), $VHH_{ZnOBP1,3}$ (*open triangles*), and $VHH_{ZnOBPtag}$ (*closed triangles*) against 0.2 mg of ZnO particles in 10 mM phosphate solution (pH 7.5; 200 mM NaCl, 0.05% Tween 20).**

that most VHH fragments have a β-structure in the center region of CDR 2 (20, 29–31). This β-structure in CDR 2 might be important for scaffold stability. We therefore analyzed the binding affinity of VHH_{ZnOBP1} and VHH_{ZnOBP3} for the ZnO surface.

To measure the ability of ZnOBP-grafted VHH fragments to bind to the ZnO surface, we measured the adsorption isotherms of VHH_{ZnOBP1} and VHH_{ZnOBP3} for ZnO particles (Fig. 3). In a phosphate solution, few cAbBCII10 VHH or VHH_{ZnOBP3} fragments were adsorbed onto ZnO particles, but, critically, VHH_{ZnOBP1} fragments were bound to ZnO particles with a dissociation equilibrium constant K_D comparable with that of VHH fragments with ZnOBP as a tag at the N terminus (VHH_{ZnOBP1}, 176 nM; $VHH_{ZnOBPtag}$, 303 nM; see Table 2): ZnOBP was as functional in CDR 1 as at the N terminus.

In addition, we grafted the ZnOBP sequence into CDR 3 of VHH_{ZnOBP1} ($VHH_{ZnOBP1,3}$) in an effort to improve the binding affinity for the ZnO surface; however, the K_D value of $VHH_{ZnOBP1,3}$ was the same as that of VHH_{ZnOBP1} (Fig. 3 and Table 2). ZnOBP in the CDR 3 loop did not function effectively even in the presence of VHH_{ZnOBP1}.

Generation of High Affinity Antibody Fragments from Peptide-grafted VHH—To improve the binding affinity of ZnOBP-grafted VHH fragments, we employed a phage-display system whereby VHH_{ZnOBP1} with the CDR 3 loop randomized was displayed on the filamentous bacteriophage M13. Evaluation of statistics on the frequency of amino acids in reported material-binding peptides selected from a phage display peptide library (5) revealed the preferential selection of Arg, His, and Lys residues among polar amino acids, and Thai *et al.* (32) have implied the presence of the Arg-Xaa-Xaa-Arg sequence in metal oxide binding. Here, we made a CDR 3 library with an αββα-repeating sequence by utilizing degenerate codes; the β residues were randomized to Arg, Gly, Leu, or Val, and the α residues were randomized to Arg or His. Lys residues could not be included in the library because of the lack of flexibility of the codons encoding Lys.

Phages displaying VHH_{ZnOBP1} with CDR 3 randomized were mixed with ZnO particles, and unbound phages were removed by the addition of 10–50 mM phosphate solution containing 0.05% Tween 20. The residual phages bound to ZnO were separated from the ZnO particles by the addition of a 200 mM phosphate solution, because highly concentrated phosphate solution can inhibit protein adsorption. We examined the frequency of amino acid residues at each position in CDR 3 among the 200 clones randomly picked from the VHH_{ZnOBP1} library, before selection and after four rounds of selection (Fig. 4). His residues were dominantly selected at the α positions, and Leu and Gly residues were concentrated at the β positions (Fig. 4*C*). To estimate the binding affinities of selected clones, we chose four clones (3D2, 3E2, 4D4, and 4F2) and measured the adsorption isotherms of each VHH (Fig. 5). All the selected VHH fragments of each clone showed higher affinity for ZnO than did

balt3/zbc-bc/zbc-bc/zbc01310/zbc0798-10z ZSUBMIT 18 xppws S=1 21/1/10 7:07 | 4/Color Figure(s) F1,4,10 | ARTNO: M109.020156

TABLE 2

Dissociation equilibrium constant (K_D) and maximum adsorption amount (W) of ZnOBP-grafted VHH fragments against ZnO

	K_D	W	Coefficient of determination[a]
	nM	nmol/m^2	
cAbBCII10 VHH	ND[b]	ND	ND
VHH_{ZnOBP1}	176	152	0.999
VHH_{ZnOBP3}	ND	ND	ND
$VHH_{ZnOBP1,3}$	165	181	0.996
$VHH_{ZnOBPtag}$	303	142	0.995

[a] Coefficient of determination is the square of correlation coefficients calculated from the fitting of Langmuir's adsorption isotherm by least square method. The value represents the degree of fitting coincidence.
[b] ND means not detected.

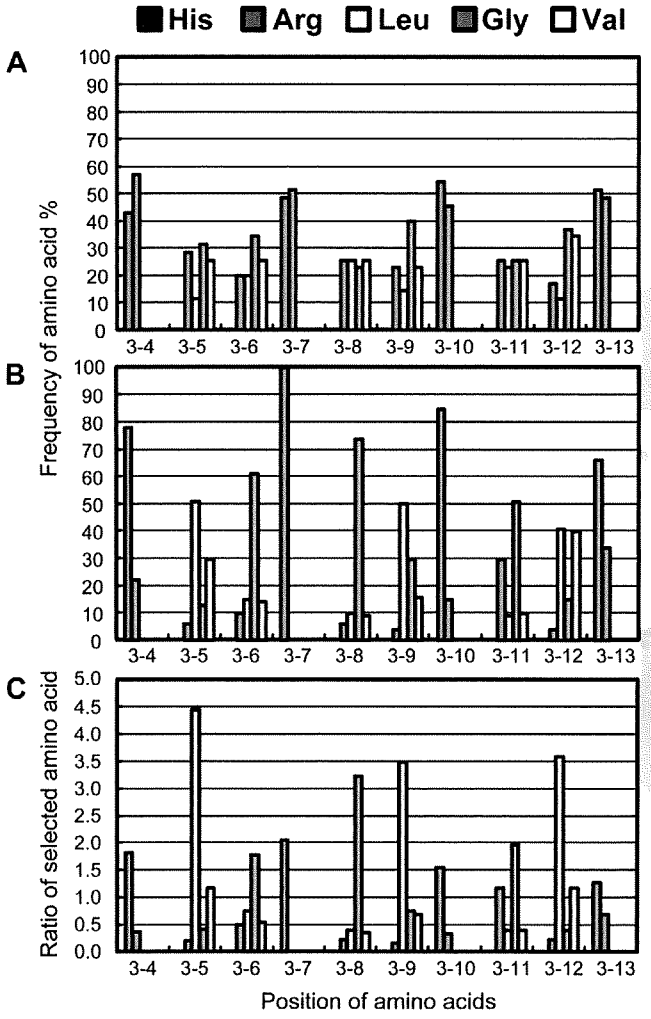

FIGURE 4. Frequencies of amino acids in randomized CDR 3 sequences of VHH_{ZnOBP1} before selection against ZnO (*A*) and after the fourth selection procedure with ZnO particles (*B*) are shown. The ratios of selected amino acids that are obtained by dividing the values in *B* by those in *A* are shown in *C*. *Color bars* are amino acids as follows: His (*blue*), Arg (*green*), Leu (*white*), Gly (*red*), and Val (*yellow*).

VHH_{ZnOBP1}; 4F2 VHH had a K_D value of 9 nM, about 20 times the affinity of VHH_{ZnOBP1} (Table 3). The binding affinity of VHH $_{ZnOBP1}$ was thus improved by optimization of the CDR 3 sequence by molecular evolutionary methods.

Binding Properties of 4F2 VHH—To evaluate the role of selected CDR 3 sequence in 4F2 VHH (sZnOBP, HLGHGLHRVH) for the binding onto the ZnO surface, we prepared the VHH fragment with CDR 1 of cAbBCII10 and CDR 3 of sZnOBP ($VHH_{sZnOBP3}$), and the binding affinity of $VHH_{sZnOBP3}$ for ZnO was measured (supplemental Fig. S1*A*). The adsorption isotherm of $VHH_{sZnOBP3}$ was adequately fitted by Langmuir adsorption isotherm equation, yielding a dissociation equilibrium constant K_D of 168 nM which is similar to that of VHH_{ZnOBP1} (supplemental Fig. S1*B*). Therefore, simultaneous binding of ZnOBP (EAHVMHKVAPRP) in CDR 1 and sZnOBP (HLGHGLHRVH) in CDR 3 is attributed to the high affinity of 4F2 VHH for the ZnO surface.

We further performed the competitive assay for the binding of VHH for ZnO surface by using the peptides of ZnOBP and sZnOBP (Fig. 6). In the competitive assay, VHH fragments were gradually dissociated from ZnO particles by increasing the concentration of the peptides in wash solution, and the dissociated VHH fragments were then analyzed by SDS-PAGE. In the mixture of ZnO particles and $VHH_{ZnOBPtag}$, the VHH fragments were dissociated from ZnO particles by the addition of ZnOBP and sZnOBP (Fig. 6*A*). Similar dissociation behavior of VHH was also observed for VHH_{ZnOBP1} and $VHH_{sZnOBP3}$ (Fig. 6, *B* and *C*). These results imply that 4F2 VHH binds onto the ZnO surface with CDR 1 and 3 loops and, furthermore, that ZnOBP and sZnOBP bind onto identical local surface structure of ZnO. In the case of 4F2 VHH, few VHH fragments were dissociated from ZnO particles by adding the peptides of ZnOBP and

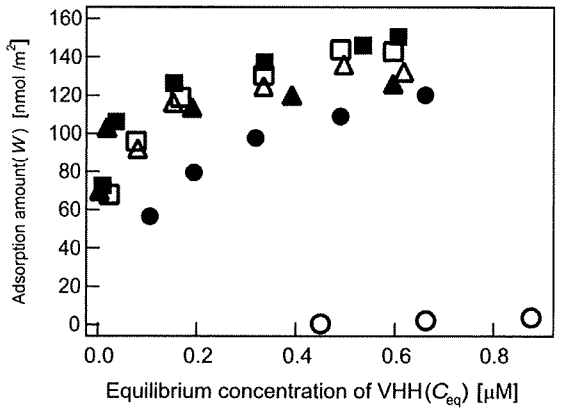

FIGURE 5. **Adsorption isotherms for cAbBCII10 VHH (*open circles*), VHH_{ZnOBP1} (*closed circles*), 3D2 VHH (*open triangles*), 3E2 VHH (*closed triangles*), 4D4 VHH (*open squares*), and 4F2 VHH (*closed squares*) against 0.2 mg of ZnO particles in 10 mM phosphate solution (pH 7.5; 200 mM NaCl, 0.05% Tween 20).**

TABLE 3

Selected VHH fragments after four rounds of selection against ZnO

Sequences selected by phage display methods are underlined. Amino acids of selected VHH are numbered as 3–1 to 3–16.

Fragment	Selected sequence in CDR3	K_D[a] [nM]	W[b] [nmol/m^2]	Coefficient of determination
	3–1 3–16			
3D2 VHH	VRGHLGHGGHRLHFRY	45	145	0.973
3E2 VHH	VRGHLGHGGHGLHFRY	21	119	0.982
4D4 VHH	VRGHVGHGLHGVRFRY	25	141	0.966
4F2 VHH	VRGHLGHGLHRVHFRY	9	139	0.977

[a] K_D is the equilibrium constant.
[b] W is the maximum adsorption amount.

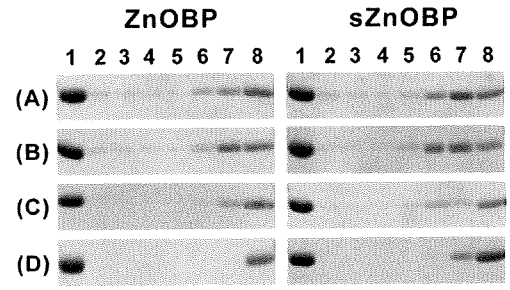

FIGURE 6. **SDS-PAGE (18% acrylamide) results of competitive inhibition assay for the binding of $VHH_{ZnOBPtag}$ (*A*), VHH_{ZnOBP1} (*B*), $VHH_{sZnOBP3}$ (*C*), and 4F2 VHH for ZnO particles with the peptides of ZnOBP and sZnOBP (*D*).** *Lanes 1–8* correspond to added VHH solution, unadsorbed fraction, wash fraction, fractions eluted with 3, 30, and 300 μM, and 3 mM peptide solutions, and fraction eluted with 6 M GdnHCl, respectively.

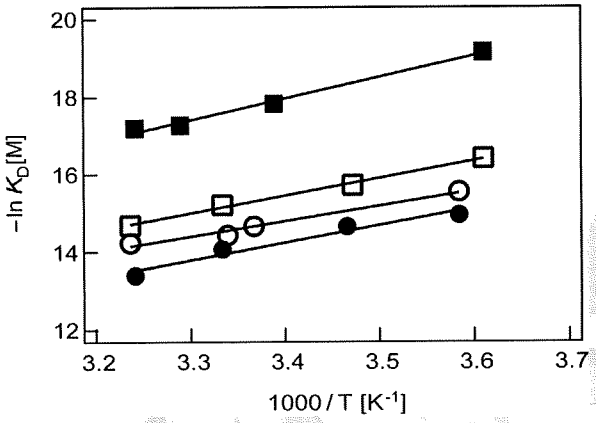

FIGURE 7. **van't Hoff plot for the binding of $VHH_{ZnOBPtag}$ (*open circles*), VHH_{ZnOBP1} (*closed circles*), $VHH_{sZnOBP3}$ (*open squares*), and 4F2 VHH (*closed squares*) to ZnO.** *Straight lines* were obtained by fitting the four points to the linearized van't Hoff equation as follows: $\ln K_D = \Delta H/RT - \Delta S/R$, where ΔH is van't Hoff enthalpy; ΔS is van't Hoff entropy, and R is universal gas constant.

TABLE 4

Thermodynamic parameters of Gibbs free energy (ΔG), enthalpy (ΔH), and entropy (ΔS) of the binding of 4F2 VHH, VHH_{ZnOBP1}, $VHH_{sZnOBP3}$, $VHH_{ZnOBPtag}$ for ZnO surface

The values were calculated from the K_D values by van't Hoff equation.

Fragment	ΔH	$T\Delta S$	$-\Delta G$
	kJ/mol	*kJ/mol*	*kJ/mol*
$VHH_{ZnOBPtag}$	−32.6	−3.6	36.2
VHH_{ZnOBP1}	−37.1	2.3	34.8
$VHH_{sZnOBP3}$	−37.3	−0.5	37.8
4F2 VHH	−45.7	−1.8	43.9

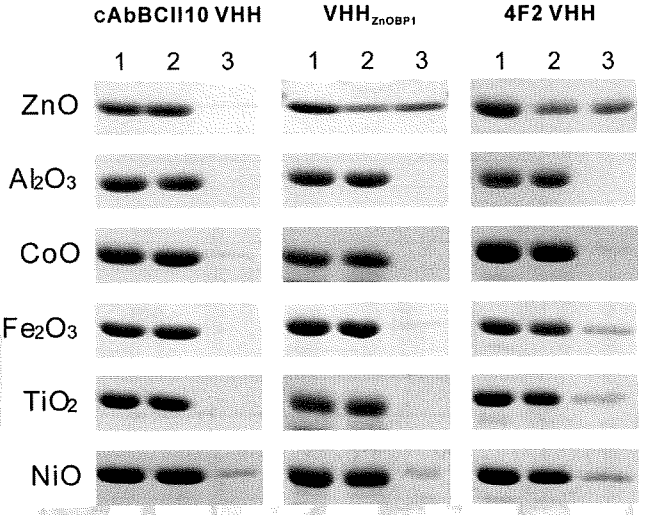

FIGURE 8. **SDS-PAGE (18% acrylamide) analysis for the selectivity of VHH against ceramics.** After the mixed solutions of each VHH (peptide-ungrafted VHH, VHH_{ZnOBP1}, or 4F2 VHH) and material particles (ZnO, Al_2O_3, CoO, Fe_2O_3, TiO_2, or NiO) had been centrifuged, the supernatant was removed, and the VHH adsorbed on the particles was eluted in 6 M GdnHCl solution. *Lane 1*, added VHH solution in particle suspension; *lane 2*, supernatant after centrifugation; *lane 3*, eluted fraction.

sZnOBP at less than 3 mM that was 1000-fold of VHH concentration (Fig. 6*D*), which supports the results from adsorption isotherm measurement that 4F2 VHH have higher affinity for ZnO than VHH_{ZnOBP1} and $VHH_{sZnOBP3}$. It should be noted that the addition of 3 mM resulted in the dissociation of 4F2 VHH. These might indicate that the peptide of sZnOBP has higher affinity for ZnO than ZnOBP.

Thermodynamic Analysis of the Interaction between VHH and ZnO—To study the thermodynamics for the interaction of ZnO-binding VHH with ZnO surface, we measured the adsorption isotherm of VHH fragments for ZnO at various temperatures. The dissociation equilibrium constants K_D estimated from the adsorption isotherm at various temperatures were plotted to the van't Hoff representation ($\ln K_D = \Delta H/RT - \Delta S/R$) (Fig. 7). The series of K_D values showed a good correlation to the van't Hoff equation for all the VHH fragments, and enthalpies and entropies were obtained from the fitting (Table 4). It should be noted that all the ZnO-binding VHH fragments of VHH_{ZnOBP1}, $VHH_{sZnOBP3}$, and 4F2 VHH had large negative enthalpy changes for the binding to ZnO. This result suggests that the interactions of all the VHH fragments with ZnO surface is derived by enthalpy factor, i.e. electrostatic interaction. Furthermore, the fact that the evolution from VHH_{ZnOBP1} to 4F2 VHH increased the negative enthalpy change implies that the improvement of binding affinity is due to the increase of electrostatic interaction between VHH and ZnO surface.

Specificity of Anti-ZnO VHH Fragments for Other Ceramic Materials—To analyze the affinity of ZnO-binding VHH fragments for other materials, we mixed VHH fragments with particles of each material. After centrifugation, the supernatant was removed, and the VHH fragments adsorbed onto particles were separated by using a 6 M GdnHCl elute solution. Fig. 8 shows the SDS-PAGE results for the supernatant and elute solution. Few peptide-ungrafted VHH fragments were adsorbed onto any ceramic particles except NiO, whereas VHH_{ZnOBP1} bound to only ZnO and NiO particles. The finding that the amount of VHH_{ZnOBP1} adsorbed onto NiO was comparable with that of peptide-ungrafted VHH indicates that the framework structure of VHH was apt to be adsorbed onto the NiO particles. Therefore, VHH_{ZnOBP1} selectively bound to ZnO via the CDR 1 loop. In the case of 4F2 VHH, few VHH fragments were bound to CoO or Al_2O_3 particles, but some were adsorbed onto Fe_2O_3 and TiO_2. However, the K_D values of 4F2 VHH for Fe_2O_3 and TiO_2 were 745 and 286 nM, respectively, indicating much lower binding affinity than for ZnO (Table 3). Therefore, the high binding ability of 4F2 VHH to ceramic materials is ZnO-specific.

balt3/zbc-bc/zbc-bc/zbc01310/zbc0798-10z ZSUBMIT 18 xppws S=1 21/1/10 7:07 | 4/Color Figure(s) F1,4,10 | ARTNO: M109.020156

TABLE 5

Selected VHH fragments after four rounds of selection against Al_2O_3 and CoO

Sequences selected by phage display methods are underlined. Numbering of the amino acids of VHH_{AlOBP1} and VHH_{CoOBP1} follows the Kabat numbering system (20). Amino acids of selected VHH are numbered as 3–1 to 3–16.

Fragment	Selected sequence in CDR 3	K_D[a] [nM]	W[b] [nmol/m^2]	Coefficient of determination
Against Al_2O_3:	95 102			
VHH_{AlOBP1}	VRGYFMRLPSSHNFRY	3100	180	0.990
	3-1 3-16			
4C5 VHH	VRGHLRHGLHLRHFRY	49	115	0.990
4D7 VHH	VRGHLGHGVHLRHFRY	220	112	0.999
4E1 VHH	VRGHLRHGLHGVRFRY	55	111	0.998
4G1 VHH	VRGHVGRGGHGLRFRY	53	127	0.997
Against CoO:	95 102			
VHH_{CoOBP1}	VRGYFMRLPSSHNFRY	1080	102	0.995
	3-1 3-16			
4B3 VHH	VRGHVVHGGHGVRFRY	140	301	0.976
4E3 VHH	VRGHLGHVRHGLRFRY	124	426	0.991
4H1 VHH	VRGRVVHGGHVGRFRY	219	299	0.990
4H12 VHH	VRGRRVHGGHGVRFRY	–[c]	–[c]	–[c]

[a] K_D is equilibrium constant.
[b] W is maximum adsorption amount.
[c] The amounts of 4H12 VHH fragments prepared by *E. coli* expression were too small to measure adsorption isotherms.

Availability of the Construction Method of Material-binding Antibodies for Other Inorganic Materials—We attempted to generate anti-Al_2O_3 VHH fragments from a reported Al_2O_3-binding peptide (KRHKQKTSRMGK) (23) and anti-CoO VHH fragments from a reported CoO-binding peptide (LGKDRPHFHRS) (24). Grafting of the peptide into the CDR 1 loop functionalized the VHH fragments. Although the peptide grafting into CDR 3 showed no functionalization, the evolutionary approach in CDR 3 critically increased the affinity for the corresponding material surface (Table 5). VHH fragments with high affinity for gold have also been generated; hence, the construction of antibody by integrating grafting and evolution technology, we call CAnIGET, can widely generate high affinity antibodies against inorganic material surfaces.

We examined the specificities of anti-Al_2O_3 4G1 and anti-CoO 4E3 VHH fragments for various materials (Fig. 9). Unlike the case with VHH_{ZnOBP1}, VHH_{AlOBP1} with Al_2O_3-binding peptide and VHH_{CoOBP1} with CoO-binding peptide in CDR 1 did not show clear specificity for each ceramic material, because of the broad material specificity of the peptides used. The finding that both the 4G1 and 4E3 VHH fragments had ambiguous material specificities implies that the material specificity of high affinity antibodies generated by construction of antibody by integrating grafting and evolution technology is strongly dependent on the characteristics of the grafted peptide.

Application of 4F2 VHH to Bio-interface Molecule—To utilize 4F2 VHH for spontaneous selective protein immobilization on a ZnO plate in a flow system, we developed a solution containing anti-ZnO VHH fragments on a ZnO film deposited on a silicon plate and detected immobilization of the protein by reflectometric interference spectroscopy (Fig. 10*A*). Under flow conditions, the time-dependent change in wavelength with minimum intensity in the reflected spectrum showed little adsorption of peptide-ungrafted VHH fragments on the ZnO film, whereas definite spontaneous immobilization of VHH_{ZnOBP1}, $VHH_{ZnOBPtag}$, and 4F2 VHH was observed, with the amounts of adsorbed protein comparable with those estimated under batch conditions (Tables 2 and 3). It should be noted that the dissociation of 4F2 VHH was too slow to be observed in the dissociation process.

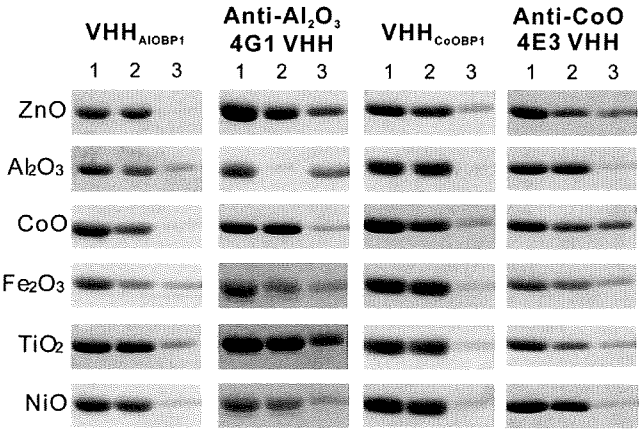

FIGURE 9. **SDS-PAGE (18% acrylamide) analysis of the selectivity of VHH_{AlOBP1}, anti-Al_2O_3 4G1 VHH, VHH_{CoOBP1}, and anti-CoO 4E3 VHH against ZnO, Al_2O_3, CoO, Fe_2O_3, TiO_2, and NiO.** After the solutions of VHH and material particles were centrifuged, the supernatant was removed, and the VHH adsorbed onto the particles was eluted with 6 M GdnHCl solution. *Lane 1*, VHH solution added to particle suspension; *lane 2*, supernatant after centrifugation; *lane 3*, eluted fraction.

Fig. 10*B* shows stepwise protein immobilization on ZnO film via bispecific VHH dimer. Bispecific VHH dimers were constructed by fusing anti-GFP VHH to the C terminus of 4F2 VHH via a hinge linker. The VHH dimers bound the surface of ZnO film with the same binding strength as 4F2 VHH, and then GFP loaded after injection of the VHH dimers was immobilized on the ZnO film. When we estimated the binding activity of each VHH domain in the bispecific dimer from the amounts of immobilized protein in Fig. 10*B*, the 4F2 VHH and anti-GFP VHH domains in the dimer retained 100 and 81% of their activity on the ZnO film; seven GFP proteins were immobilized on a 100-nm^2 area. The conservation of the activity of both VHH domains and the high rates of occupancy of the ZnO film by GFP indicate that the bispecific VHH dimer format with the high affinity material-binding antibody fragment was effective as a bio-interface molecule for direct and easy immobilization of proteins.

DISCUSSION

Single Domain Camel VHH Fragment as a Framework for Grafting Material-binding Peptide—The structural resemblance of human and mouse Fv frameworks enables the transfer of binding function to humanized antibodies (33); these replacement techniques are currently applied to the design of new functional antibody fragments by the grafting of alien

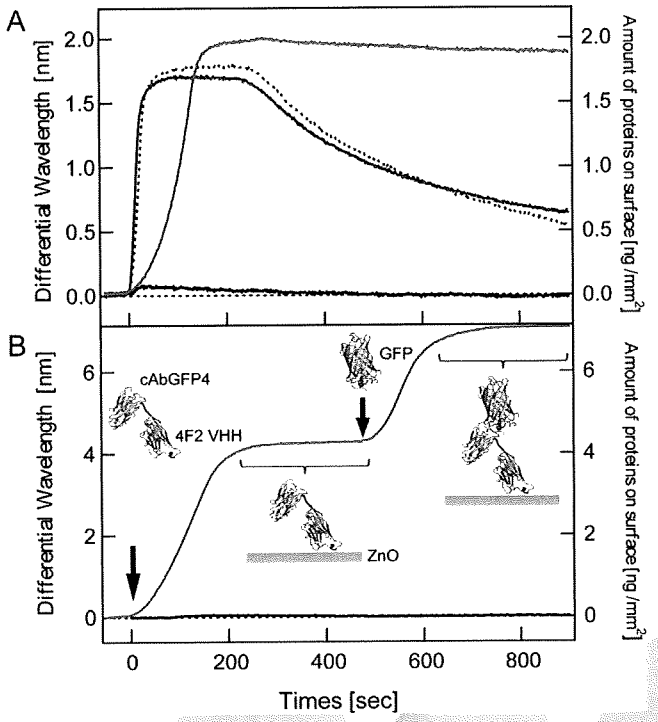

FIGURE 10. **Spontaneous stepwise-stacking of proteins on ZnO via 4F2 VHH.** *A*, reflectometric interference sensorgrams for interaction of 4F2 VHH (*red, solid line*), VHH_{ZnOBP1} (*blue, solid line*), $VHH_{ZnOBPtag}$ (*blue, dotted line*), and cAbBCII10 VHH (*black, solid line*) with ZnO film. Each VHH solution (1 μM) was injected for 240 s. *B*, reflectometric interference sensorgram (*red, solid line*) of the interaction of bispecific VHH dimers with ZnO film and GFP. VHH dimer solution (1 μM) was injected for 240 s, after which time GFP proteins were injected. *Arrow* indicates the timing of GFP injection. *Black line* corresponds to the sensorgram measured when only GFP proteins were injected for 240 s.

motif peptide sequences (34–36). Previously, we functionalized an Fv fragment from mouse anti-lysozyme antibody HyHEL-10 by grafting material-binding peptides into the heavy chain CDR 2 region (22); however, the replacement caused dissociation of the Fv fragment. The framework used did not have enough structural versatility for the grafting of material-binding peptide sequences.

Here, we used the variable fragment from a camel antibody, cAbBCII10 VHH, as a new framework for the grafting of material-binding peptide. The cAbBCII10 VHH fragment is a single domain with a framework tolerant to various CDR loop structures (20). cAbBCII10 VHH was also an appropriate stable framework for the replacement of CDRs 1 and 3 with material-binding peptides, although grafting into the CDR 3 loop did not functionalize VHH. Our previous study of the Fv fragment suggested the importance of the exposure of grafted material-binding peptide by means of a scaffold (22); however, the CDR 1 and 3 loops are sufficiently exposed in the reported crystal structure of cAbBCII10 VHH (31). The general VHH fragment recognizes an antigen by using the CDR 1 and 3 loops (37); in particular, CDR 3 has a greater variety of length and conformation than other CDRs, and the variety generates a single-domain VHH equal in binding affinity to heterodimer Fv. The length and conformational variety of CDR 3 are accompanied by the interaction of CDR 3 with frameworks and CDR 1, which controls the orientation of CDR 3 to give high binding affinity (38). In this study, our grafting design for CDR 3 might have yielded an improper conformation of ZnOBP, *i.e.* grafting into CDR 3 might have required more careful design. Our results demonstrate that CDR 3 should be functionalized by molecular evolution rather than by peptide grafting.

Affinity Maturation of ZBP-grafted VHH by Molecular Evolution in CDR 3—There have been a few studies of the selection of antibodies with affinity for material surfaces by using general methodologies with *in vivo* immune systems (15) or *in vitro* library methods (16–19). However, because of the low immunogenic potential of solid materials, far fewer antibodies with affinities for material surfaces have been selected than those with affinities for soluble molecules. Even with the use of *in vitro* selection methods, the limited library diversity and strong nonspecific interactions of coat proteins on phages with solid bulk surfaces make it difficult to select positive antibodies. We demonstrated here the possibility of steadily generating high affinity antibodies by coupling the grafting of peptides from a reported material-binding peptide repertoire and molecular evolution of the peptide-grafted variable fragment. The construction of a library from a low affinity antibody for which the binding site could be predicted allowed us to narrow down the segments that needed to be randomized, thus enabling us to bypass the limitations of library diversity.

Randomization of the CDR 3 loop in the format of the $\alpha\beta\beta\alpha$ repeating sequence can also decrease the necessary magnitude of library diversity. The $\alpha\beta\beta\alpha$ format was designed in consideration of the Arg-Xaa-Xaa-Arg format (32), the importance of His residues for inorganic material binding (39), and the frequent appearance of Arg, His, and Lys residues in material-binding peptides. Use of the $\alpha\beta\beta\alpha$ format with Arg/Gly/Leu/Val at the β positions and His/Arg at the α positions resulted in the preferential selection of Gly/Leu (β) and His (α) in the selection of VHH against ZnO. Notably, few Arg residues were selected at both the β and α positions. These results suggest that in CDR 3 in the VHH scaffold, Arg has less functional ability than His to bind to the ZnO surface.

Synergistic Effect of CDR Loops on Binding on the ZnO Surface—In this study, we focused the binding properties of the highest affinity 4F2 VHH fragment. The comparison with VHH_{ZnOBP1} and $VHH_{sZnOBP3}$ indicates that the high binding affinity of 4F2 VHH resulted from synergistic effect from grafted CDR 1 and selected CDR 3 loops in the VHH framework (Fig. 6). The competitive binding assay by using the peptides of ZnOBP and sZnOBP implied that CDR 1 and CDR 3 recognized identical local surface structure of ZnO.

To increase the affinity of the peptides with micromolar K_D values, repetition and clustering of material-binding peptides are among the possible approaches to increasing the binding affinity of peptides that have micromolar K_D values (3). One polypeptide with three repeats of a gold-binding peptide had a K_D value of 89 nM (40), and clustering of 24 titania-binding peptides on a ferritin protein increased the binding affinity, giving a K_D value of 11 nM (41). Our high affinity antibody fragments showed strong binding with only two loop structures (CDRs 1 and 3). Therefore, use of the antibody format has the

potential for efficient generation of high affinity interface molecules from material-binding peptides.

Thermodynamic Analysis for the Binding of Anti-ZnO VHH to ZnO Surface—The thermodynamic parameters estimated from van't Hoff plots demonstrated dominant change of enthalpy in the absorption process of all the ZnO-binding VHH fragments ($VHH_{ZnOBPtag}$, VHH_{ZnOBP1}, $VHH_{sZnOBP3}$, and 4F2 VHH) on the ZnO surface. This result is comparable with the binding properties of anti-gold antibody Fv fragment, A14P-b2 Fv (18). This implies that coulombic interaction dominates the binding process of anti-ZnO VHH fragments on ZnO. Considering that ZnO surface and the framework of VHH are positively charged at the pH value of 7.5, the grafted and selected CDR loops electrostatically interact with the ZnO surface. In general, one of major factors for protein adsorption on material surface is entropy changes that result from dehydration of the absorbent surface and from the conformational change of adsorbed proteins (42, 43). Therefore, our thermodynamic result implies that the conformation of anti-ZnO VHH fragments is little changed by interaction with the ZnO surface and that few water molecules on ZnO surface are dispersed by the binding of VHH. When the CD spectra were measured on 4F2 VHH fragments with ZnO nanoparticles, we observed the CD spectra derived from the immunoglobulin structure of camel antibody (data not shown). Hence, 4F2 VHH was not denatured on the ZnO surface.

Application of High Affinity Antibody Fragment for Nanobiotechnology—Antibody fragments are among the smallest units with naturally occurring binding domains, and an advantage of using them as high affinity interface molecules is the fact that various fusion technologies can be used. Artificial antibody formats constructed for therapeutic and imaging uses have been used to generate multivalent and multispecific material-binding antibodies to functionalize nanoparticles and to spontaneously and selectively accumulate proteins and nanoparticles on patterned spots on substrate (18, 44). Here, we show the potential of high affinity material-binding antibodies for selective immobilization of proteins on biosensor plates. The fusion of material-binding peptides and antibody fragments enables direct and oriented protein immobilization without the need for complicated processes (9, 45), and unmodified inorganic surfaces can directly receive electrons from immobilized redox proteins without mediators (46). Improving the binding strength of material-binding biomolecules will lead to more quantitative and reliable detection.

In conclusion, we generated antibody fragments with high affinity for inorganic material surfaces from low affinity material-binding peptides by the integration of peptide-grafting and phage-display techniques. The scaffold of the single-domain VHH fragment was so stable that VHH was directly functionalized by grafting of the material-binding peptide into CDR 1 without structural destabilization. Application of the $\alpha\beta\beta\alpha$ motif library to the CDR 3 of peptide-grafted VHH enabled us to bypass limitations on library diversity; consequently, this construction method allow us to generate high affinity antibodies against material surfaces from previously identified material-binding peptides. Quantitative thermodynamic analysis described the enthalpy synergistic effect from grafted and selected CDR loops in VHH, which shows the potential of antibody scaffold for creating high affinity small interface units with efficient binding mechanism. Use of the high affinity antibody fragments resulted in stable selective protein immobilization on material surfaces in flow systems. We expect to be able to use such material-binding antibodies as biointerface units for nanoscale quantitative biosensing and protein accumulation.

REFERENCES

1. Carvalho, A. L., Goyal, A., Prates, J. A., Bolam, D. N., Gilbert, H. J., Pires, V. M., Ferreira, L. M., Planas, A., Romão, M. J., and Fontes, C. M. (2004) *J. Biol. Chem.* **279,** 34785–34793
2. Itoh, Y., Kawase, T., Nikaidou, N., Fukada, H., Mitsutomi, M., Watanabe, T., and Itoh, Y. (2002) *Biosci. Biotechnol. Biochem.* **66,** 1084–1092
3. Brown, S. (1997) *Nat. Biotechnol.* **15,** 269–272
4. Whaley, S. R., English, D. S., Hu, E. L., Barbara, P. F., and Belcher, A. M. (2000) *Nature* **405,** 665–668
5. Sarikaya, M., Tamerler, C., Jen, A. K., Schulten, K., and Baneyx, F. (2003) *Nat. Mater.* **2,** 577–585
6. Mao, C., Solis, D. J., Reiss, B. D., Kottmann, S. T., Sweeney, R. Y., Hayhurst, A., Georgiou, G., Iverson, B., and Belcher, A. M. (2004) *Science* **303,** 213–217
7. Naik, R. R., Stringer, S. J., Agarwal, G., Jones, S. E., and Stone, M. O. (2002) *Nat. Mater.* **1,** 169–172
8. Tamerler, C., Duman, M., Oren, E. E., Gungormus, M., Xiong, X., Kacar, T., Parviz, B. A., and Sarikaya, M. (2006) *Small* **2,** 1372–1378
9. Park, T. J., Lee, S. Y., Lee, S. J., Park, J. P., Yang, K. S., Lee, K. B., Ko, S., Park, J. B., Kim, T., Kim, S. K., Shin, Y. B., Chung, B. H., Ku, S. J., Kim do, H., and Choi, I. S. (2006) *Anal. Chem.* **78,** 7197–7205
10. Brown, S. (2001) *Nano Lett.* **1,** 391–394 AQ: B
11. Umetsu, M., Mizuta, M., Tsumoto, K., Ohara, S., Takami, S., Watanabe, H., Kumagai, I., and Adschiri, T. (2005) *Adv. Mater.* **17,** 2571–2575 AQ: C
12. Kramer, R. M., Li, C., Carter, D. C., Stone, M. O., and Naik, R. R. (2004) *J. Am. Chem. Soc.* **126,** 13282–13286
13. Adams, G. P., and Weiner, L. M. (2005) *Nat. Biotechnol.* **23,** 1147–1157
14. Kessler, N., Perl-Treves, D., and Addadi, L. (1996) *FASEB J.* **10,** 1435–1442
15. Geva, M., Frolow, F., Eisenstein, M., and Addadi, L. (2003) *J. Am. Chem. Soc.* **125,** 696–704
16. Barbas, C. F., 3rd, Rosenblum, J. S., and Lerner, R. A. (1993) *Proc. Natl. Acad. Sci. U.S.A.* **90,** 6385–6389
17. Artzy Schnirman, A., Zahavi, E., Yeger, H., Rosenfeld, R., Benhar, I., Reiter, Y., and Sivan, U. (2006) *Nano Lett.* **6,** 1870–1874
18. Watanabe, H., Nakanishi, T., Umetsu, M., and Kumagai, I. (2008) *J. Biol. Chem.* **283,** 36031–36038
19. Watanabe, H., Tsumoto, K., Taguchi, S., Yamashita, K., Doi, Y., Nishimiya, Y., Kondo, H., Umetsu, M., and Kumagai, I. (2007) *Bioconjug. Chem.* **18,** 645–651
20. Saerens, D., Pellis, M., Loris, R., Pardon, E., Dumoulin, M., Matagne, A., Wyns, L., Muyldermans, S., and Conrath, K. (2005) *J. Mol. Biol.* **352,** 597–607
21. Sato, K., Tsuchiya, M., Saldanha, J., Koishihara, Y., Ohsugi, Y., Kishimoto, T., and Bendig, M. M. (1994) *Mol. Immunol.* **31,** 371–381
22. Hattori, T., Umetsu, M., Nakanishi, T., Tsumoto, K., Ohara, S., Abe, H., Naito, M., Asano, R., Adschiri, T., and Kumagai, I. (2008) *Biochem. Biophys. Res. Commun.* **365,** 751–757
23. Krauland, E. M., Peelle, B. R., Wittrup, K. D., and Belcher, A. M. (2007) *Biotechnol. Bioeng.* **97,** 1009–1020
24. Schembri, M. A., Kjaergaard, K., and Klemm, P. (1999) *FEMS Microbiol. Lett.* **170,** 363–371
25. Maenaka, K., Furuta, M., Tsumoto, K., Watanabe, K., Ueda, Y., and Kumagai, I. (1996) *Biochem. Biophys. Res. Commun.* **218,** 682–687
26. Brunauer, S., Emmett, P. H., and Teller, E. (1938) *J. Am. Chem. Soc.* **60,** 309–319
27. Rothbauer, U., Zolghadr, K., Tillib, S., Nowak, D., Schermelleh, L., Gahl, A., Backmann, N., Conrath, K., Muyldermans, S., Cardoso, M. C., and Leonhardt, H. (2006) *Nat. Methods* **3,** 887–889
28. Conrath, K. E., Lauwereys, M., Galleni, M., Matagne, A., Frère, J. M.,

Kinne, J., Wyns, L., and Muyldermans, S. (2001) *Antimicrob. Agents. Chemother.* **45,** 2807–2812
29. Decanniere, K., Desmyter, A., Lauwereys, M., Ghahroudi, M. A., Muyldermans, S., and Wyns, L. (1999) *Structure* **7,** 361–370
30. Conrath, K., Vincke, C., Stijlemans, B., Schymkowitz, J., Decanniere, K., Wyns, L., Muyldermans, S., and Loris, R. (2005) *J. Mol. Biol.* **350,** 112–125
31. Vincke, C., Loris, R., Saerens, D., Martinez-Rodriguez, S., Muyldermans, S., and Conrath, K. (2009) *J. Biol. Chem.* **284,** 3273–3284
32. Thai, C. K., Dai, H., Sastry, M. S., Sarikaya, M., Schwartz, D. T., and Baneyx, F. (2004) *Biotechnol. Bioeng.* **87,** 129–137
33. Jones, P. T., Dear, P. H., Foote, J., Neuberger, M. S., and Winter, G. (1986) *Nature* **321,** 522–525
34. Barbas, C. F., 3rd, Languino, L. R., and Smith, J. W. (1993) *Proc. Natl. Acad. Sci. U.S.A.* **90,** 10003–10007
35. Moroncini, G., Kanu, N., Solforosi, L., Abalos, G., Telling, G. C., Head, M., Ironside, J., Brockes, J. P., Burton, D. R., and Williamson, R. A. (2004) *Proc. Natl. Acad. Sci. U.S.A.* **101,** 10404–10409
36. Frederickson, S., Renshaw, M. W., Lin, B., Smith, L. M., Calveley, P., Springhorn, J. P., Johnson, K., Wang, Y., Su, X., Shen, Y., and Bowdish, K. S. (2006) *Proc. Natl. Acad. Sci. U.S.A.* **103,** 14307–14312
37. Muyldermans, S. (2001) *J. Biotechnol.* **74,** 277–302
38. Muyldermans, S., and Lauwereys, M. (1999) *J. Mol. Recognit.* **12,** 131–140
39. Peelle, B. R., Krauland, E. M., Wittrup, K. D., and Belcher, A. M. (2005) *Langmuir* **21,** 6929–6933
40. Tamerler, C., Oren, E. E., Duman, M., Venkatasubramanian, E., and Sarikaya, M. (2006) *Langmuir* **22,** 7712–7718
41. Sano, K., Ajima, K., Iwahori, K., Yudasaka, M., Iijima, S., Yamashita, I., and Shiba, K. (2005) *Small* **1,** 826–832
42. Norde, W., and Lyklema, J. (1978) *J. Colloid Interface Sci.* **66,** 257–265
43. Norde, W., and Lyklema, J. (1979) *J. Colloid Interface Sci.* **71,** 350–366
44. Umetsu, M., Hattori, T., Kikuchi, S., Muto, I., Nakanishi, T., Watanabe, H., and Kumagai, I. (2008) *J. Mater. Sci.* **23,** 3241–3246
45. Woodbury, R. G., Wendin, C., Clendenning, J., Melendez, J., Elkind, J., Bartholomew, D., Brown, S., and Furlong, C. E. (1998) *Biosens. Bioelectron* **13,** 1117–1126
46. Habermüller, K., Mosbach, M., and Schuhmann, W. (2000) *Fresenius J. Anal. Chem.* **366,** 560–568

ASBMB

JBC Papers in Press. Published on December 28, 2009 as Manuscript M109.089623
The latest version is at http://www.jbc.org/cgi/doi/10.1074/jbc.M109.089623

CONTRIBUTION OF ASPARAGINE RESIDUES TO THE STABILIZATION OF A PROTEINACEOUS ANTIGEN-ANTIBODY COMPLEX: HyHEL-10–HEL

Akiko Yokota[1,2], Kouhei Tsumoto[1,3#], Mitsunori Shiroishi[1], Takeshi Nakanishi[1], Hidemasa Kondo[4], and Izumi Kumagai[1†]

[1]Department of Biomolecular Engineering, Graduate School of Engineering, Tohoku University, Aoba-yama 6-6-11, Sendai 980-8579, Japan,[2]Protein Design Research Group, Institute for Biological Resources and Functions, National Institute of Advanced Industrial Science and Technology (AIST), 1-1-1, Higashi, Tsukuba, Ibaraki 305-8566, Japan,[3]Department of Medical Genome Sciences, Graduate School of Frontier Sciences, The University of Tokyo, Kashiwa 277-8562, Japan,[4]Functional Protein Research Group, Research Institute of Genome-based Biofactory, National Institute of Advanced Industrial Science and Technology (AIST), 2-17-2-1 Tsukisamu-Higashi, Toyohira, Sapporo 062-8517, Japan

Running head: Asparagine in a proteinaceous antigen-antibody complex

To whom correspondence may be addressed: E-mail: tsumoto@k.u-tokyo.ac.jp.

† To whom correspondence may be addressed. E-mail: kmiz@kuma.che.tohoku.ac.jp

Many germline antibodies have asparagine residues at specific sites to achieve specific antigen recognition. To study the role of asparagine residues in the stabilization of antigen-antibody complexes, we examined the interaction between hen egg white lysozyme (HEL) and the corresponding HyHEL-10 variable domain fragment (Fv). We introduced Ala and Asp substitutions into the Fv side chains of L-Asn31, L-Asn32 and L-Asn92, which interact directly with residues in HEL via hydrogen bonding in the wild-type Fv–HEL complex, and investigated the interactions between these mutant antibodies and HEL. Isothermal titration calorimetric analysis showed that all the mutations decreased the negative enthalpy change and decreased the association constants of the interaction. Structural analyses showed that the effects of the mutations on the structure of the complex could be compensated for by conformational changes and/or by gains in other interactions. Consequently, the contribution of two hydrogen bonds was minor, and their abolition by mutation resulted in only a slight decrease in the affinity of the antibody for its antigen. By comparison, the other two hydrogen bonds buried at the interfacial area, had large enthalpic advantage, despite entropic loss that was perhaps due to stiffening of the interface by the bonds, and were crucial to the strength of the interaction. Deletion of these strong hydrogen bonds could not be compensated for by other structural changes. Our results suggest that asparagine can provide the two functional groups for strong hydrogen bond formation, and their contribution to the antigen-antibody interaction can be attributed to their limited flexibility and accessibility at the complex interface.

The specific recognition of ligands by proteins is a fundamental biological phenomenon (1), and the interaction between antigen and antibody in the immune system is a typical example. Antibodies acquire their affinity and specificity for various target antigens by changing the amino acid residue

Copyright 2009 by The American Society for Biochemistry and Molecular Biology, Inc.

Downloaded from www.jbc.org at TOHOKU UNIVERSITY, on January 27, 2010

composition of their six hyper-variable regions, known as complementarity-determining regions (CDRs) (2). Despite the small number of amino acid residues composing the CDRs, antibodies can precisely bind a large number of target antigens (3). Some of these residues, for example, serine and asparagine, are located at specific positions in the CDRs in the germline protein (Supplemental Fig. S1). Many structural studies have shown that these residues are essential for the affinity and specificity of the antigen-antibody interaction (4-11).

Recent high-resolution analyses of three-dimensional structures of protein-ligand complexes, including the antigen-antibody complexes, and analyses of the kinetic and thermodynamic parameters underlying these interactions (12-19), have indicated that protein-ligand interactions require a good geometric fit according to the lock-and-key (20) and induced fit models (21) as well as a high degree of complementarity of hydrophobic and polar parts of each binding site (17, 22, 23). There are various forces determining the affinity and specificity of these interfacial complementarities including non-covalent bonds, such as hydrogen bonds, salt bridges and van der Waals interactions (17, 22-24). Among of those non-covalent bonds, hydrogen bonds play a unique and functionally important role in molecular associations because of its involvement in both thermodynamic and kinetic processes. Firstly, hydrogen bonds are strong and directional enough to control and direct the structures within molecular assemblies. Secondly, from a mechanistic point of view, the energy of hydrogen bonds, which is between that of van der Waals interactions and covalent bonds, allows biomolecules to associate and dissociate quickly at room temperature. These features of hydrogen bonds form the basis by which specific recognition is achieved quickly with moderate affinity (25). Many studies show that hydrogen bonds play a significant role in a wide range of biomolecular interactions in terms of generating affinity and specific recognition (26-31). It is also reported that hydrogen bonds can make a favorable enthalpic contribution to protein-ligand interactions (32-34). Thus, the subject of hydrogen bonding is of major interest in biological research.

Here, we investigated the involvement of side chains of asparagine and serine in hydrogen bond formation. To elucidate the contribution of hydrogen bonds to the affinity and specificity of antigen-antibody interactions, mutagenesis in combination with both structural and thermodynamic analyses has been a productive and powerful strategy (35). X-ray crystallographic studies can provide information on the structural complementary of the mutant antibody (or antigen) and its interaction with its counterpart (36-39), and measurement of thermodynamic parameters can quantify the energetic effect of the mutated residues on the interaction (40, 41). Approaches based on multiple analyses are essential to further our understanding of the mechanisms underlying the roles of hydrogen bonds in antigen-antibody interactions.

We focused on the interaction between hen egg white lysozyme (HEL) and the variable domain fragment (Fv) of the anti-HEL monoclonal antibody HyHEL-10, which is one of the most studied proteinaceous antigen-antibody interactions in terms of structural and functional features (42-50). The bacterial expression system for

Downloaded from www.jbc.org at TOHOKU UNIVERSITY, on January 27, 2010

the HyHEL-10 Fv fragment has been established (51-53), and the Fv–HEL interactions have been investigated by using the wild type and/or mutant Fv fragments (42-44, 46, 47, 54), including the X-ray crystal structure of its complex with HEL (45, 47, 48, 55). In the wild-type Fv–HEL complex, Kondo *et al.* (45) observed 12 water molecules bridging the imperfect antigen-antibody interface as well as 20 direct hydrogen bonds between residues of the antibody and antigen at the interface. In a previous study, we examined the role of indirect hydrogen bonds via interfacial water molecules in the HyHEL-10 Fv–HEL interaction by thermodynamic analysis and X-ray structural analysis in combination with mutagenesis (48). We discovered that hydrogen bonds made a minor contribution by providing an enthalpic advantage to the interaction, despite the partial offset caused by entropy loss resulting from the hydrogen bonding stiffening the antigen-antibody complex (48). Here, we further examined the role of hydrogen bonds in stiffening the antigen-antibody complex by focusing on the three residues Asn31, Asn32, and Asn92 in the light chain, which have side-chain amide groups that participate in the formation of direct hydrogen bonds with residues in HEL (Fig. 1). Mutational analyses achieved by truncating these amide groups in the antibody side chains should give further insight into the effect of direct hydrogen bonding on complex formation. We constructed six Fv mutants, L-Asn31Asp, L-Asn31Ala, L-Asn32Asp, L-Asn32Ala, L-Asn92Asp, and L-Asn92Ala, and performed thermodynamic analyses of the interaction between these HyHEL-10 Fv mutants and HEL by means of isothermal titration calorimetry (ITC) in combination with X-ray crystallographic analysis of the mutant Fv–HEL complexes. Based on our results, we elucidated the contribution of direct hydrogen bonds at the atomic level to the antigen-antibody interaction. We also discussed the role of interfacial asparagine residues in the antigen-antibody interaction with respect to their role in achieving specificity and affinity of antibodies for target antigens.

EXPERIMENTAL PROCEDURES

Materials— All enzymes for genetic engineering were obtained from Takara Shuzo (Kyoto, Japan), Toyobo (Osaka, Japan), and New England Biolabs (Beverly, MA, USA). Isopropyl-β-D-thiogalactopyranoside was obtained from Wako Fine Chemicals Inc. (Osaka, Japan). All other reagents were of biochemical research grade. The HEL antigen purchased from Seikagaku-Kogyo, Tokyo, Japan, was purified by ion exchange chromatography on SP-Sepharose FF (GE Healthcare, Tokyo, Japan), followed by gel filtration on Superdex 75 pg equilibrated with phosphate-buffered saline. Eluted antigen was lyophilized and dissolved in water at a concentration of 0.54 mM prior to use.

Site-directed Mutagenesis— The gene structure of the light chain variable region (VL) and heavy chain variable region (VH) coexpression vector of the HyHEL-10 Fv fragment is described in our previous paper (51). Site-directed mutagenesis was performed with phagemid pTZ18U (Bio-Rad, Laboratories, Inc., Tokyo, Japan) according to the method of Kunkel *et al.* (56). The DNA oligonucleotide primers for mutation of Asn to Ala, and Asn to Asp, at sites 31, 32 and 92 of VL were
5'-GTCGATCGGCGCCAACCTCCAC-3',
5'-GTCGATCGGCGACAACCTCCAC-3',

Downloaded from www.jbc.org at TOHOKU UNIVERSITY, on January 27, 2010

5'-GATCGGCAACGCCCTCCACTGG-3',
5'-GATCGGCAACGACCTCCACTGG-3',
5'-CAGCAGTCGGCCAGCTGGCCG-3' and
5'-CAGCAGTCGGACAGCTGGCCG-3',
respectively (mutated sites are underlined). The correctness of the intended mutations was confirmed by DNA sequencing (ABI 310 Genetic Analyzer, Applied Biosystems, Tokyo, Japan).

Preparation of HyHEL-10 Mutant Fv fragments— We obtained wild-type and mutant Fv fragments by using the *Escherichia coli* BL21 (DE3) expression system. BL21 (DE3) cells harboring the appropriate expression plasmid were precultured in 3 mL of LB medium, which was then used to innoculate in 3 L of 2× YT medium containing 100 μg/L ampicillin. The culture was shaken overnight at 28°C, centrifuged at 3000 × *g* for 20 min, and the bacteria pallet was resuspended in 3 L of 2× YT medium containing 100 μg/L ampicillin and isopropyl 1-thio-β-D-galactopyranoside at a final concentration of 1 mM. The culture was again shaken overnight at 28°C. The culture was then centrifuged at 3000 × *g* for 20 min and the collected supernatant was subjected to ammonium sulfate precipitation at 80% saturated ammonium sulfate, followed by centrifugation. The protein pellet was solubilized in 30–40 mL of PBS buffer and then dialyzed against PBS buffer. Fv fragments were purified by affinity chromatography. The protein solution was loaded onto an HEL-Sepharose column (51), and the column was washed with PBS buffer and then wash buffer (50 mM Tris-HCl, pH 8.5, containing 0.5 M NaCl). Fv fragments were eluted with elution buffer (0.1 M Gly-HCl, pH 2.0, containing 0.2 M NaCl) and then buffered rapidly with 1 M Tris-HCl (pH 7.5). Fv-containing fractions were centrifuged, and minor impurities were removed by gel filtration with a Sephacryl S-200 column (GE Healthcare) pre-equilibrated with 50 mM Tris-HCl (pH 7.5) containing 0.2 M NaCl. The purity of isolated proteins was confirmed by SDS-PAGE in the buffer system described by Laemmli (57). The purified Fv fragments were concentrated using a Centriprep-10 column (Millipore, Bilerica, MA, USA).

Inhibition Assay of HEL Enzymatic Activity— The experimental procedure for the inhibition assay was essentially as described by Ueda *et al.* (51). Briefly, various concentrations of the Fv fragment were mixed with 1.5 μM HEL and incubated at 25°C for 1 h in 30 μL of phosphate-buffered saline. Each mixture was then added to 970 μL of 50 mM NaH_2PO_4 buffer (pH 6.2, adjusted with NaOH) containing 340 μg of *Micrococcus luteus* cells. The initial rate of the decrease in $A_{540\ nm}$ was monitored at 25°C.

Isothermal Titration Calorimetry— Thermodynamic parameters of the interaction between HEL and wild-type or mutant HyHEL-10 Fv fragments were determined by ITC using a VP-ITC microcalorimeter (MicroCal, Inc., Northampton, MA). HEL at 5 μM in 50 mM phosphate buffer (pH 7.2) containing 0.2 M NaCl, was placed into the calorimeter cell and was titrated with a 50 μM solution of the Fv fragment in the same buffer at four different temperatures (25°C, 30°C, 35°C, or 40°C) for the LN31A, LN31D, LN32D and LN92D mutants, and at one temperature (30°C) for the LN32A mutant. The solution containing the Fv fragments was injected 25 times in 10 μL aliquots over 20 s. Thermograms were analyzed with Origin 5 software (MicroCal, Inc.) after correcting for the buffer contribution. The enthalpy change

Downloaded from www.jbc.org at TOHOKU UNIVERSITY, on January 27, 2010

(ΔH) and binding constant (K_a) for each antigen-antibody interaction were obtained directly from the experimental titration curve. The Gibbs free energy change ($\Delta G = -RT \ln K_a$) and the entropy change ($\Delta S = (-\Delta G + \Delta H)/T$) for the association were calculated from the ΔH and K_a. The heat capacity change (ΔC_p) was estimated from the temperature dependence of the enthalpy change.

Estimation of Protein Concentration— The concentration of HEL was estimated by using $A^{1\%}_{280} = 26.5$ (58). The concentrations of wild type and mutant HyHEL-10 Fv fragments were estimated by using $A^{1\%}_{280} = 20.6$ (51).

Crystallization, Data Collection, and Structural Determination of the HyHEL-10 Mutant Fv-HEL Complexes— Fv fragment–HEL complexes for the three HyHEL-10 mutants LN31D, LN32D, and LN92D were crystallized under conditions similar to those used for the wild-type Fv–HEL complex (45). The best crystals were grown in 0.1 M Hepes buffer (pH 7.6–7.8), 9–11% w/v polyethylene glycol 6000, and 7–9% (w/v) 2-methyl-2,4-pentanediol. The resultant crystals were elongated bipyramid shapes. For the LN31A–HEL complex, a micro needle-like crystal was obtained in 0.1–0.2 M ammonium sulfate, 22.5–27.5% w/v polyethylene glycol 4000, and 0.1–0.2 M sodium acetate trihydrate (pH 4.6); however, it was too small to be used for obtaining data sets of X-ray diffraction images. Furthermore, for the LN32A–HEL complex, the sample of LN32A Fv fragment was too poor to crystallize. All crystallization conditions included glycerol at a final concentration of 15% as a cryoprotectant.

Data sets for all mutant Fv–HEL complexes were obtained at 100 K using the synchrotron X-ray source at beamline BL6A at the Photon Factory (Tsukuba, Japan). The diffraction images were processed by the interactive data processing package DPS/MOSFLM/CCP4. Integration was carried out using the MOSFLM software (59); scaling was carried out using SCALA software (60), and the final file of structural factors was obtained by using TRUNCATE (61) and MTZ2VARIOUS in the CCP4 program suite (62). The structures of the Fv–HEL complexes were determined by a molecular replacement method using the wild-type complex (Protein Data Bank ID code 2DQJ) as a model structure, and refined by using the CNS program (63). The graphic program O (64) was used for making adjustments to the molecular model. Crystallographic and refinement data for each Fv mutant–HEL complex are summarized in the Supplemental Table S1.

Calculations of the root-mean-square deviation (RMSD) for structural comparison were performed using the programs LSQKAB (65) and COMPAR in the CCP4 software suite. Interfacial areas were calculated with AREAIMOL in the CCP4 software suite. Determination of contacting atoms between Fv and HEL was performed with the CONTACT program in the CCP4 suite. Figures were drawn with the program WebLab Viewer Lite (Accelrys Inc., San Diego, CA, USA).

Atomic coordinates and structural factors for each mutant Fv–HEL complex were deposited in the Protein Data Bank. The Protein Data Bank accession codes are 3A67 for LN31D, 3A6B for LN32D, and 3A6C for LN92D.

RESULTS

Downloaded from www.jbc.org at TOHOKU UNIVERSITY, on January 27, 2010

Expression and Purification of Fv fragments— To elucidate the role of interfacial asparagine residues in direct hydrogen bond formation in HyHEL-10 Fv–HEL complexes, we constructed, expressed and purified six mutant Fv fragments named LN31A, LN31D, LN32A, LN32D, LN92A, and LN92D. With the exception of LN32A and LN92A, we obtained purities of greater than 95% and the final yields were greater than 10 mg/L of culture. LN92A could not be expressed using the established expression system. Furthermore, the yield of LN32A was low following purification, despite the level of expression, thus only a limited number of experiments were performed for LN32A.

Inhibition of Enzymatic Activity of Hen Lysozyme by Mutant Fv fragments— Tsumoto and co-workers (42, 51, 52) demonstrated that the HyHEL-10 Fv fragment inhibits the enzymatic activity of its antigen, HEL, in the presence of a slight molar excess of the Fv fragment. Thus, we investigated the inhibition of the enzymatic activity of HEL by the wild-type Fv fragment and the five of the mutant Fv fragments LN31A, LN31D, LN32A, LN32D, and LN92D (Fig. 2). The wild-type Fv fragment and LN31D showed a similar level of inhibition of HEL enzymatic activity and for LN92D this level was only slightly lower than that of the wild type. By comparison, the level of inhibition of HEL enzymatic activity shown by LN32D was notably lower than that of the wild type. LN31A and LN32A displayed no inhibitory activities toward HEL. These results suggest that the mutations harbored by LN31A, LN32A, and LN32D play an important role in target antigen affinity.

Thermodynamic Analyses— To investigate the interactions between the Fv fragment mutants and HEL from a thermodynamic viewpoint, we carried out an ITC study of the association between the mutant Fv fragments and lysozyme (42-44, 46-48, 55). The thermogram for each experiment was obtained by titrating the HEL solution with the Fv solution and then subtracting the baseline obtained from titrating buffer with the Fv solution (Fig. 3). Thermodynamic parameters are summarized in Table 1. In the Asp substitution mutants LN31D (L-Asn31) and LN92D (L-Asn92), thermodynamic analysis revealed that a small loss in binding enthalpy ($\Delta\Delta H$, 6.9 kJ mol^{-1} for LN31D and $\Delta\Delta H$, 5.1 kJ mol^{-1} for LN92D) and a smaller (near to zero) gain in binding entropy led to a minor loss in Gibbs energy of binding compared with the wild type-HEL interaction, and resulted in a small decrease in the binding affinity constants for LN31D (K_a, 17.8×10^7 M^{-1}) and LN92D (K_a, 14.0×10^7 M^{-1}). By comparison, for LN31A, LN32A, and LN32D, there was a large decrease in negative binding enthalpy and there was a decrease in binding entropy loss, which notably decreased the Gibbs energy of binding. These results indicated that the interaction between HEL and each Ala or Asp substitution in the Fv fragments at L-Asn31, L-Asn32 and L-Asn92, led to unfavorable enthalpy changes and favorable entropy changes, and that the enthalpy-entropy compensation reduced the loss in the Gibbs energy change, to some degree. For LN31A, LN32A, and LN32D, the large decrease in enthalpy change failed to maintain affinity for HEL, resulting in marked 600-fold, 500-fold, and 100-fold decreases in their binding affinity constant, respectively, compared to that of the wild type. The change in heat capacity for LN31A, LN31D,

Downloaded from www.jbc.org at TOHOKU UNIVERSITY, on January 27, 2010

LN32D, and LN92D, estimated from the values of enthalpy change of temperature dependency, were −2.35, −1.70, −1.01, and −1.68 kJ mol^{-1} K^{-1}, respectively (Supplemental Fig. S2).

Crystal Structure of Mutant Fv–HEL Complexes— The crystal structures of mutant HyHEL-10 Fv–HEL complexes were solved at resolutions sufficient for determining local structural differences (1.8 Å) (Supplemental Table S1). Most of the interfacial water molecules, which mediate the Fv–HEL interaction, were conserved among the mutant Fv–HEL and wild-type complexes (Supplemental Table S2). Additional interfacial water molecules appear in the LN32D–HEL and LN92D–HEL complexes.

Crystal structures of mutant HyHEL-10 Fv–HEL complexes were superimposed onto the wild-type Fv–HEL complex by means of the LSQKAB (65) and COMPER programs in the CCP4 software suite (62). The resultant RMSD between C-α atoms of each mutant–HEL complex and that of the wild-type Fv–HEL complex, are shown in Table 2. The structure of the LN31D–HEL complex is similar to that of the wild-type Fv–HEL complex, apart from the region containing 17–19 residues in HEL adjacent to its epitope, which is out of alignment in the other mutant Fv–HEL complexes (48). The crystal structure of the LN32D–HEL and LN92D–HEL complexes is relatively distinct from that of the wild-type Fv–HEL complex. In LN32D–HEL and LN92D–HEL, the RMSD value for each polypeptide obtained by superposing the corresponding polypeptide, and the RMSD value for the Fv fragment obtained by superposing Fv chains, are very low. These observations indicate that the Asp substitution at L-Asn32 and L-Asn92 did not introduce drastic structural changes to the respective domains. However, the RMSD values for VL and/or VH, in the case of HEL-fitting, and the RMSD values for HEL, in the case of Fv-fitting, especially for the L-Asn32 Fv–HEL complex, are moderately large. This finding shows that the orientation of VL and/or VH (in other words, Fv) with HEL in the LN32D–HEL and LN92D–HEL complexes is different to that in the wild-type Fv–HEL complex, and that the difference in relative orientation of VL, VH, and HEL in the LN32D–HEL complex is greater than that in the LN92D–HEL complex (Table 2).

The interfacial areas within the crystal structures of mutant HyHEL-10 Fv–HEL complexes were calculated by means of the program AREAMOL in the CCP4 software suite and are listed in Supplemental Table S3. In LN32D–HEL and LN92D–HEL, the total interfacial area is reduced mostly because of a decrease in the VL–HEL interfacial area, whereas in LN31D–HEL the domains (VL, VH, and HEL) and total interfacial area are similar to those in the wild-type Fv–HEL complex.

The direct contacts between mutant HyHEL-10 Fv and HEL in the mutant complexes were calculated by means of the program CONTACT in the CCP4 software suite (Supplemental Table S4). In LN31D–HEL, the non-covalent bonds were well-conserved with the wild-type Fv–HEL complex. By comparison, in the LN32D and LN92D–HEL complexes, multiple non-covalent bonds, which were largely distinct from those in the wild-type Fv–HEL complex, were observed. Hydrogen bonds and van der Waals interactions between CDR-L3 and HEL were abolished. Four hydrogen bonds between CDR-H1 and

Downloaded from www.jbc.org at TOHOKU UNIVERSITY, on January 27, 2010

CDR-H2 and HEL, multiple van der Waals contacts, and one salt bridge between CDR-H3 and CDR-L3 and HEL, were newly introduced and increased the total number of interactions in the LN32D–HEL and LN92D–HEL complexes. These contact changes (loss and/or gain) (Supplemental Table S5) and the subsequent local structural changes at the mutated sites (Fig. 4) are similar in the LN32D–HEL and LN92D–HEL complexes.

Our results have lead to the following conclusions: 1) the overall structure of LN31D–HEL, including its interfacial region, that is the size of interfacial area, formations of atomic contacts and interfacial water molecules, is almost identical to that of the wild-type Fv–HEL complex; 2) in LN32D–HEL and LN92D–HEL, the relative orientation of Fv (VL and VH) and HEL was notably altered by the mutations, resulting in the structure of the interfacial regions being different to that in the wild-type Fv–HEL complex; 3) the structural differences in LN32D–HEL and LN92D-HEL are similar, except for the hydrogen bonds generated by the amide group of the mutated side chains in LN32D and LN92D.

Structure of Mutant Fv–HEL Complexes

LN31D–HEL— The overall structure of LN31D–HEL, including the interfacial water molecules, and the local structure around the site of mutation, is similar to that of the wild-type Fv–HEL complex (Table 2, Supplemental Table S2, S3, S4 and S5 and Fig. 4a). The structures of antigen-antibody interfacial sites, other than the site of mutation, are also similar to that of the wild-type complex. Thus, the removal of hydrogen bond between Nδ2 in L-Asn31 and O in His15 of HEL, resulting from the substitution of L-Asn31 with Asp, has little impact on the antigen-antibody interaction.

LN32D–HEL— The backbone structure of LN32D–HEL was in principle identical to the corresponding structure in the wild-type Fv–HEL complex. However, the relative orientation of VL, VH and HEL was altered in the mutant complex. In particular, the difference in the orientation of Fv and HEL between the wild-type and LN32D complexes is great (Table 2), as described above. In addition, the local structures within the LN32D complex, especially at the antigen-antibody interface, are notably different from those in the wild-type complex (Table 2, Supplemental Table S2, S3, S4 and S5, and Fig. 4B). Notably, the atoms of Oδ2 in L-Asp32 and of O in HEL-Gly16, which were originally close enough to create a hydrogen bond in the wild-type complex, are widely separated from each other in the mutant complex because of indirect hydrogen bonds from a newly introduced interfacial molecular water (W34) located between them. Furthermore, within the same proximity as the mutated site, conformational changes were observed around multiple residues in LN32D and around the counterpart residues in HEL including L-Asn31 and His15, because of newly formed hydrogen bonds between Oδ1 in L-Asn31 and O in HEL-His15. Therefore, around the mutated site of L-Asp32 in LN32D–HEL, in which the target hydrogen bond was removed by the Asn to Asp substitution, the distance between L-Asp32 and HEL-Gly16 was increased thus resulting in many large structural changes, including the newly introduced interfacial water molecule, movement of interfacial water molecules, and the associated reorganization of interactions.

LN92D–HEL— In LN92D–HEL,

Downloaded from www.jbc.org at TOHOKU UNIVERSITY, on January 27, 2010

the relative orientation of VL, VH, and HEL, in particular Fv and HEL, as well as the local structure around the site of mutation, are notably different from those in the wild-type complex and similar to those in LN32D–HEL (Table 2, Supplemental Table S2, S3, S4 and S5). The local conformational changes in LN92D–HEL around the site of mutation, such as the movement of side chains and water molecules show a greater difference to those of the wild-type complex than do those in LN32D–HEL (Fig. 4C). However, differences in the RMSD and interfacial areas between the wild-type complex and LN92D–HEL were smaller than those between the wild-type complex and LN32D–HEL. The atoms of Oδ2 in L-Asp92 and of O in HEL-Asn19, which were originally close enough to create a hydrogen bond in the wild-type complex, were widely separated from each other in LN92D–HEL. A similar situation was observed for Oδ2 in L-Asp32 and for O in HEL-Gly16 in LN32D–HEL. The removal of direct hydrogen bonds resulted in conformational changes in the surrounding region and resulted in a newly introduced interfacial water molecule (W57), movement of multiple water molecules, and the reconstruction of interfacial hydrogen bonding networks accompanying these changes.

Comparison between LN32D–HEL and LN92D–HEL— The local conformational changes around L-Asn92 in LN32D–HEL (Fig. 5A) are similar to those in LN92D–HEL, especially in the characteristic movement of the side chain of Asn19 in HEL that interacts with L-Asn92 (Fig. 4C). The local conformational changes around L-Asn31 and L-Asn32 in LN92D–HEL (Fig. 5B) are similar to those in LN32D–HEL in terms of their effects on the surrounding region, including a newly introduced interfacial water molecule at the coordinate W95, which corresponds to W34 in LN32D–HEL, movement of multiple water molecules, and the reconstruction of interfacial hydrogen bonding networks accompanying these changes. Thus, the only difference between the LN92D–HEL and LN32D–HEL complexes is the substantial conformational change resulting from the maintenance of the hydrogen bond between Nδ2 of L-Asn32 and O of HEL-Gly16 in the LN92D–HEL complex that is not present in the LN32D–HEL complex.

DISCUSSION

Here, we constructed six mutant HyHEL-10 Fv fragments named LN31A, LN31D, LN32A, LN32D, LN92A, and LN92D to elucidate the energetic contributions of direct (not via interfacial water molecules) hydrogen bonds, which are formed by amino acid residues in antibody-antigen interactions. We investigated the interactions between mutant Fv fragments and the HEL antigen by structural and thermodynamic analyses of the resultant complexes. The mutations do not lead to drastic structural changes of the Fv fragments, with the exception of LN92A, and do not alter their stability. Thus, the structural and thermodynamic changes we observed in the mutant antigen-antibody complexes do not originate from changes in the structure of the mutant Fv fragments in the antigen-free state. However, a slight and minor change in the structure of the antigen-free Fv fragment might have a strong impact on the interaction between the Fv fragment and the antigen. To address this, it is necessary to investigate the structural changes in the Fv fragment in the

Downloaded from www.jbc.org at TOHOKU UNIVERSITY, on January 27, 2010

antigen-free state; structural analyses of antigen-free Fv will be reported in the near future (T. N. and I. K., manuscript in preparation). In the following sections, we discuss and correlate our thermodynamic and structural findings.

Thermodynamic Analysis of Mutant Fv–HEL Interactions— The values for the enthalpic ($-\Delta H$) and entropic ($-T\Delta S$) contributions to the interaction between the mutants and HEL increased in the order LN92D, LN31D, LN32A, LN31A, and LN32D. The values of the binding constant (K_a) for the LN31D–HEL and LN92D–HEL interactions were slightly lower than that for the wild-type Fv–HEL interaction, whereas the K_a for the LN31A–HEL, LN32A–HEL and LN32D–HEL interactions were markedly lower than that for the wild-type Fv–HEL interaction, resulting in a smaller change in the Gibbs energy ($-\Delta G$). These results indicate that removal of the direct hydrogen bonds formed through interfacial Asn residues on the light chain of the antibody in the HyHEL-10 Fv–HEL complex is enthalpically unfavorable and entropically favorable. Thus, the interfacial hydrogen bonds appeared to make an enthalpic contribution to the HyHEL-10 Fv–HEL interaction similar to the finding in a previous study for indirect hydrogen bonds via interfacial water molecules (48). For the LN31A–HEL, LN32A–HEL, and LN32D–HEL interactions, the advantage in binding entropy relative to that in the wild type cannot compensate for the loss in binding enthalpy and so causes a decrease in their affinities compared to the wild-type interaction.

We estimated the change in heat capacity change (ΔC_p), from the temperature dependence of the enthalpy changes for interactions between LN31A, LN31D, LN32D, and LN92D, and the antigen. The ΔC_p values for the interactions between LN31D and LN92D and HEL (−1.70 kJ mol^{-1} and −1.68 kJ mol^{-1}, respectively) were similar to that for the interaction between the wild type and HEL (−1.53 kJ mol^{-1}), whereas those for the LN31A–HEL and LN32D–HEL interactions were lower (−2.35 kJ mol^{-1}) and greater (−1.01 kJ mol^{-1}), respectively, than the wild-type Fv–HEL interaction. It has been reported that the large negative heat capacity change is related to the decrease in the non-polar accessible surface area (ΔASA_{apolar}) for water molecules, *i.e.*, the hydrophobic effect of the molecule association (66-69). The ΔC_p values for the LN31A–HEL and LN32D–HEL interactions suggest that the conformational changes and/or hydration structure changes introduced by the interaction of the mutant antibodies with HEL could be different to those introduced in the wild-type Fv–HEL interaction (68, 70, 71).

L-Asn31: contribution of the polar but non-charged side chain is favorable for the interaction— The overall structure, the size of interfacial area, formations of atomic contacts, position of interfacial water molecules, and the local structure around the mutation site of the LN31D–HEL complex are similar to that of the wild-type complex (Table 2 and Supplemental Table S2, S3, S4 and S5, and Fig. 4A). These results suggested that the effects of the loss of hydrogen bonds caused by the substitution of L-Asn31 with Asp on the interaction between the mutant Fv and HEL are directly reflected in the changes to the thermodymamic parameters (ΔG, ΔH, ΔS, and ΔC_p) (Table 1). Thermodynamically, the substitution of L-Asn31 with Asp leads to

Downloaded from www.jbc.org at TOHOKU UNIVERSITY, on January 27, 2010